Hindawi
Advances in Meteorology
Volume 2019, Article ID 9098576, 8 pages
https://doi.org/10.1155/2019/9098576

Research Article

Solar Radiation Partitioning and Surface Albedo Parameterization in the Hinterland of Taklimakan Desert

Chunlei Meng[1] **and Huoqing Li**[2]

[1]*Institute of Urban Meteorology, China Meteorological Administration, 100089 Beijing, China*
[2]*Institute of Desert Meteorology, China Meteorological Administration, 830002 Urumqi, Xinjiang, China*

Correspondence should be addressed to Chunlei Meng; clmeng@ium.cn

Received 15 July 2019; Accepted 21 November 2019; Published 11 December 2019

Academic Editor: Helena A. Flocas

Surface albedo is one of the key parameters of land surface radiation and energy balance. As surface albedoes for visible and near-infrared solar radiation are quite different, solar radiation partitioning is important to parameterize the total surface albedo and upward solar radiation. In this paper, a surface albedo parameterization scheme was introduced and a solar radiation partitioning method was developed to improve the simulation of the upward solar radiation. The simulation results were validated in a hinterland site of the Taklimakan Desert. The surface albedo is not only associated with the soil moisture, but associated with the solar zenith angle. The solar radiation partitioning method considers the joint influences of cloud cover, near-surface air pressure, and solar zenith angle and was compared with the method using the Simple Biosphere Model version 3 (SiB3). The total albedo depends on the partitioning of the total visible and near-infrared radiations. The results indicate the surface albedo parameterization scheme is important to parameterize the upward solar radiation. The new solar radiation partitioning method could improve the simulation result.

1. Introduction

Surface albedo is defined as the surface reflected solar radiation divided by the surface incident solar radiation. It is one of the key parameters of land surface radiation [1] and energy balance [2, 3] and shapes the earth's climate and climate change [4–14]. In arid and semiarid regions, such as the Taklimakan Desert, as the fractional vegetation cover is relatively low, the surface albedo is an important parameter in land surface temperature variation [15] and hence has impact on the atmospheric circulation [16] and water cycle. As a result, the surface albedo is an important parameter in aridification [17] and desertification [18] for arid and semiarid land surfaces.

Some land surface models such as the Common Land Model (CoLM) [19] only consider the effect of soil color and soil moisture on surface albedo parameterization. Many research results [20–27] show that surface albedo is not only associated with the soil moisture and soil color, but also associated with the solar zenith angle. In addition, surface albedo is also associated with the wave length of solar radiation [28, 29]. The albedo for near-infrared solar radiation is usually larger than that for visible solar radiation. As the surface albedoes for visible and near-infrared solar radiation are quite different, solar radiation partitioning is important to parameterize the total surface albedo and the upward solar radiation. Weiss and Norman [30] partitioned the clear day solar radiation into four parts based on Bouguer's Law, i.e., the direct visible, diffuse visible, direct near-infrared, and diffuse near-infrared solar radiation. These four parts of solar radiation are associated with the solar zenith angle and the near-surface air pressure. In the Simple Biosphere Model version 3 (SiB3) [31–33], these four parts of solar radiation are associated with the cloud cover.

In this paper, Zheng's [29] method was introduced to the integrated urban land model (IUM) [34] to parameterize the surface albedo for bare soil in arid and semiarid areas. A solar radiation partitioning method was developed based on [30]. In order to expand the applicability of the solar radiation partitioning method to all weather conditions, the effect of cloud cover was considered in the solar radiation partitioning method. Both the surface albedo parameterization scheme and the solar radiation partitioning method

were validated by comparing with the observed upward solar radiation in a hinterland site of the Taklimakan Desert.

2. Data and Method

2.1. Study Site. Taklimakan Desert is located in Central Asia; it is the second biggest desert in the world. The precipitation of the Taklimakan Desert is extremely scarce, and the climate is extremely dry. The land cover of the Taklimakan Desert is relatively single. The fractional vegetation cover is very low. The Taklimakan Desert atmospheric environment observation experimental station (Tazhong station) is located in the hinterland of the Taklimakan Desert. The altitude is 1099.3 m and the longitude and latitude are 83.650 E and 38.967 N, respectively (Figure 1).

2.2. Data. The observational data from the Tazhong station are used to initialize and drive the land surface model and validate the surface albedo and solar radiation partitioning method. The turbulent heat fluxes including the sensible heat flux and the latent heat flux are measured using the eddy covariance (EC) technique at 80 meter height. The radiation fluxes including the upward and downward shortwave and longwave radiation are measured using the Kipp & Zonen CNR-1 net radiometer. The observed upward shortwave radiation data are used to validate the simulation results. The simulation time period is a whole year of 2014. The temporal resolution of the simulation is 30 min.

2.3. Land Surface Model. The IUM [34] was developed based on the Common Land Model (CoLM) [19]. As an integrated land model, IUM integrates the urban land model with the common land model. For the natural land surface, IUM was developed based on CoLM. A whole layer soil evaporation parameterization scheme was developed to improve the simulation of soil evaporation especially in arid areas. For the urban land surface, the energy and water balance model were modified; urban land surface parameters such as the anthropogenic heat (AH), albedo, surface roughness length, and imperious surface evaporation were also reparameterized. A mosaic scheme was applied in order to maximize the use of the high-resolution land use and land cover (LULC) data.

2.4. Method

2.4.1. Surface Albedo. The solar radiation partitioning and surface albedo parameterization method in the IUM are both the same as those in the CoLM. The surface albedo is defined as follows [19]:

$$\alpha = \frac{\left(\alpha_{\text{vis,dif}} + \alpha_{\text{nir,dif}}\right)}{2}, \tag{1a}$$

$$\alpha_{\text{nir,dif}} = 2 \cdot \alpha_{\text{vis,dif}}, \tag{1b}$$

where α is the surface albedo and $\alpha_{\text{vis,dif}}$ and $\alpha_{\text{nir,dif}}$ are the surface albedoes for visible and near-infrared diffuse solar radiation, respectively. For bare soil, they are associated with the soil wetness and the soil color.

In this paper, the surface albedo parameterization scheme is from [29]. The surface albedo is not only associated with the soil wetness, but also associated with the solar elevation angle. For bare soil in arid and semiarid areas, surface albedo could be parameterized as follows:

$$\alpha_{\text{vis,dif}} = 0.22 \times \left[1 + \exp\left(-0.15 \times h_\theta\right)\right] - 0.45 \times \theta, \tag{2a}$$

$$\alpha_{\text{nir,dif}} = 0.26 \times \left[1 + \exp\left(-0.15 \times h_\theta\right)\right] - 0.45 \times \theta, \tag{2b}$$

$$\alpha_{\text{vis,dir}} = \alpha_{\text{vis,dif}}, \tag{2c}$$

$$\alpha_{\text{nir,dir}} = \alpha_{\text{nir,dif}}, \tag{2d}$$

where h_θ is the solar elevation angle (°), θ is the volumetric soil moisture, and $\alpha_{\text{vis,dir}}$ and $\alpha_{\text{nir,dir}}$ are the albedoes for visible and near-infrared direct solar radiation, respectively.

2.4.2. Solar Radiation Partitioning. In the IUM, the solar radiation is divided into two equal parts, namely, the visible and near-infrared diffuse radiation. In theory, solar radiation could be divided into six parts: they are visible, near-infrared, and ultraviolet direct and diffuse radiation. The percentage of ultraviolet radiation is relatively small and could be neglected. The visible and near-infrared radiation are associated with the solar zenith angle, the cloud fraction, and the near-surface air pressure. In this paper, the solar partitioning method is based on [30]. The four components of solar radiation could be partitioned as follows:

$$R_{\text{dv}} = 600 \times \exp\left[\frac{-0.185 \times \left(P/P_0\right)}{\cos\left(Z_\theta\right)}\right] \times \cos\left(Z_\theta\right), \tag{3a}$$

$$R_{\text{fv}} = 0.4 \times \left(600 - R_{\text{dv}}\right) \times \cos\left(Z_\theta\right), \tag{3b}$$

$$R_{\text{dn}} = \left\{720 \times \exp\left[\frac{-0.06 \times \left(P/P_0\right)}{\cos\left(Z_\theta\right)}\right] - w\right\} \times \cos\left(Z_\theta\right), \tag{3c}$$

$$R_{\text{fn}} = 0.6 \times \left(720 - R_{\text{dn}} - w\right) \times \cos\left(Z_\theta\right), \tag{3d}$$

where R_{dv}, R_{fv}, R_{dn}, and R_{fn} are the direct visible, diffuse visible, direct near-infrared, and diffuse near-infrared solar radiation (W m^{-2}), respectively; P is the near-surface air pressure (Pa); P_0 is the sea surface air pressure (Pa), which is 101,325 Pa; Z_θ is the solar zenith angle (°); and w is the water absorption in the near-infrared for 10 mm of precipitable water (W m^{-2}), which could be calculated as follows:

$$w = 1320 \times \text{anti}\log_{10}\left\{-1.1950 + 0.4459 \times \log_{10}\left[\left(\cos\left(Z_\theta\right)\right)^{-1}\right] - 0.0345 \times \left[\log_{10}\left(\left(\cos\left(Z_\theta\right)\right)^{-1}\right)\right]^2\right\}. \tag{4}$$

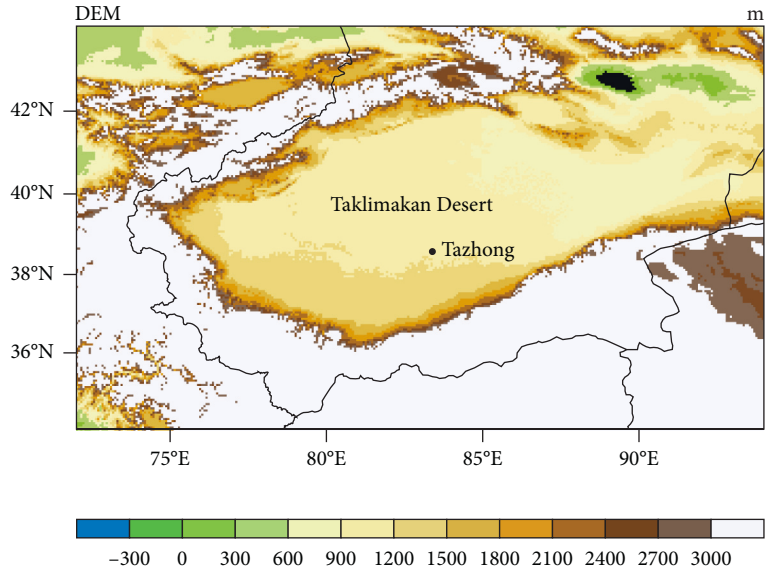

Figure 1: Location of the Tazhong station in the Taklimakan Desert.

Weiss and Norman's method is only suitable for clear sky condition. In order to expand the applicability to all weather conditions, the method was corrected to consider the effect of cloud cover. As the cloud cover increases, the percentage of the diffuse solar radiation increases and the percentage of the direct solar radiation decreases. The correction coefficients are calculated as follows:

$$C_V = \frac{(R_{dv} + R_{dn})}{R \times R_{cloud}} \times \frac{R_{fv}}{(R_{fv} + R_{fn})}, \tag{5a}$$

$$C_N = \frac{(R_{dv} + R_{dn})}{R \times R_{cloud}} \times \frac{R_{fn}}{(R_{fv} + R_{fn})}, \tag{5b}$$

where C_V and C_N are the correction coefficients for visible and near-infrared radiation, respectively, R is the total solar radiation (W m^{-2}), and R_{cloud} is the cloud fraction, which could be calculated as follows [31–33]:

$$R_{cloud} = \frac{[1160 \times \cos(Z_\theta) - R]}{[963 \times \cos(Z_\theta)]}, \quad 0 \le R_{cloud} \le 1. \tag{6}$$

After considering the correction coefficients, the four components of solar radiation could be calculated as follows:

$$R_{dvn} = R_{dv} - C_V, \tag{7a}$$

$$R_{fvn} = R_{fv} + C_V, \tag{7b}$$

$$R_{dnn} = R_{dn} - C_N, \tag{7c}$$

$$R_{fnn} = R_{fn} + C_N, \tag{7d}$$

where R_{dvn}, R_{fvn}, R_{dnn}, and R_{fnn} are the direct visible, diffuse visible, direct near-infrared, and diffuse near-infrared solar radiation (W m^{-2}) after considering the correction coefficients, respectively.

In order to evaluate the solar radiation partitioning method, it is compared with the method used in Simple Biosphere Model version 3 (SiB3) [31–33]. For the SIB3, the solar radiation partitioning is based on the cloud cover and the solar zenith angle, which could be calculated as follows:

$$R_{dv} = (1 - P_f) \times P_v \times R, \tag{8a}$$

$$R_{dn} = (1 - P_f) \times (1 - P_v) \times R, \tag{8b}$$

$$R_{fv} = P_f \times P_v \times R, \tag{8c}$$

$$R_{fn} = P_f \times (1 - P_v) \times R, \tag{8d}$$

where P_V and P_f are the percentages for visible and diffuse radiation, respectively. They could be calculated as follows:

$$P_v = \frac{(580 - R_{cloud} \times 464)}{[(580 - R_{cloud}) \times 499]} + (580 - R_{cloud} \times 464), \tag{9a}$$

$$P_f = R_{cloud} + (1 - R_{cloud}) \times \left[\frac{0.0604}{(\cos(Z_\theta) - 0.0223}\right] + 0.0683. \tag{9b}$$

After considering the solar radiation partitioning, the upward shortwave radiation should be parameterized as follows:

$$S\uparrow = \left(R_{dvn} \times \alpha_{vis,dir} + R_{dnn} \times \alpha_{nir,dir} + R_{fvn} \times \alpha_{vis,dif} + R_{fnn} \times \alpha_{nir,dif}\right) \times R, \tag{10}$$

where $S\uparrow$ is the upward solar radiation (W m^{-2}). The total surface albedo is calculated as follows:

$$\alpha = R_{dvn} \times \alpha_{vis,dir} + R_{dnn} \times \alpha_{nir,dir} + R_{fvn} \times \alpha_{vis,dif} + R_{fnn} \times \alpha_{nir,dif}. \tag{11}$$

2.4.3. Experiments Design. Four sets of experiments were designed to perform the simulation of the IUM (Table 1). Experiment one is the control run, and the default IUM was used in this experiment. For experiment two, only the new surface albedo parameterization scheme was used. For experiment three, both the new surface albedo parameterization scheme and solar partitioning method in SiB3 were used. For experiment four, both the new surface albedo parameterization scheme and the new solar partitioning method were used.

3. Results and Discussion

First, we compared the default and the new surface albedo parameterization schemes. Figure 2 shows the annual averaged diurnal cycles of the visible and near-infrared surface albedoes simulated by the default and the new surface albedo parameterization schemes. As the soil moisture has little change during the diurnal cycle period, the default surface albedoes have little change; the near-infrared surface albedo is twice as much as the visible surface albedo (equation (1b)). The new surface albedoes are relatively high in the morning and at dusk because at these times, the solar zenith angles are relatively large. The near-infrared surface albedo is less than twice of the visible surface albedo; the ratios between the near-infrared surface albedo and the visible surface albedo are almost 1.2.

Then, we compared the new solar partitioning method with the method based on [30] (Figure 3). After considering the effect of cloud cover, the diffuse visible and near-infrared radiations are increased and the direct visible and near-infrared radiations are decreased. From equations (7a)–(7d), the total visible and near-infrared radiations remain unchanged. As the total albedo only depends on the partitioning of the total visible and near-infrared radiations (equations (2a)–(2d)), the upward solar radiation has no relation with the cloud fraction. Then, we compared the new solar partitioning method with the method based on SiB3 (Figure 4(a)). For the new solar partitioning method, the diffuse visible and near-infrared radiations are both decreased and the direct visible and near-infrared radiations are both increased. We also compared the total visible and near-infrared radiations for these two solar partitioning methods (Figure 4(b)). For the SiB3-based solar partitioning method, the total visible solar radiation is larger than the total near-infrared solar radiation for the whole diurnal cycle period. On the contrary, for the new solar partitioning method, the total visible solar radiation is smaller than the total near-infrared solar radiation for the whole diurnal cycle period. As the near-infrared surface albedo is larger than the visible surface albedo, it could be deduced that the total albedo based on the SiB3 solar partitioning method is smaller than that based on the IUM default solar partitioning method. On the contrary, the total albedo based on the new solar partitioning method is larger than that based on the IUM default solar partitioning method.

To evaluate the surface albedo and solar radiation partitioning method, we compared the upward solar radiation simulation results for these four sets of experiments with those of the observations for the whole year (Figure 5). Table 2 lists the statistical variables of the upward solar radiation simulated by these four sets of experiments compared with those of the observations for the whole year.

Table 1: Experiments' design.

	Surface albedo	Solar partitioning
Set 1 (control run)	Default scheme	No
Set 2	New scheme	No
Set 3	New scheme	SiB3
Set 4	New scheme	New method

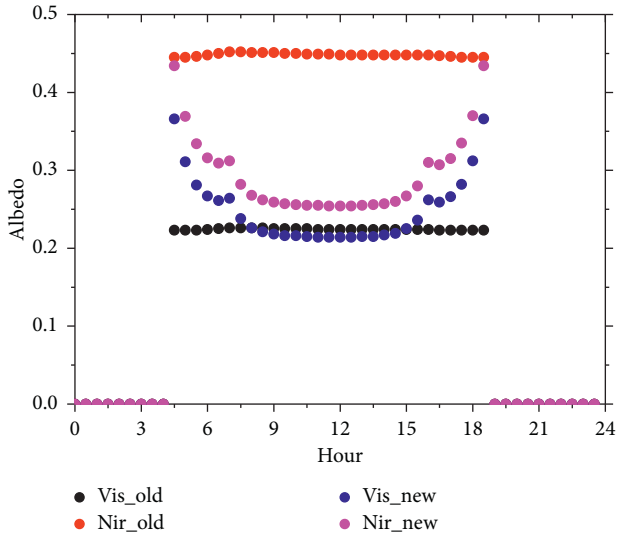

Figure 2: Comparison of the annual averaged diurnal cycle of the visible and near-infrared surface albedoes between the default and the new surface albedo parameterization schemes.

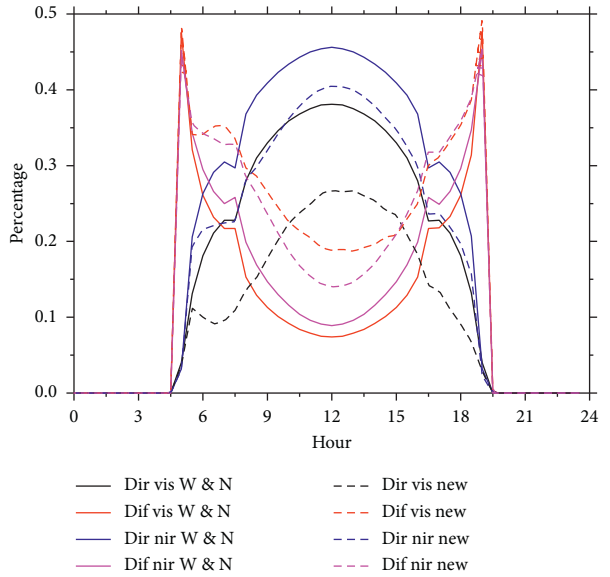

Figure 3: Comparison of the annual averaged diurnal cycle of the solar radiation partitioning between Weiss and Norman and the new surface albedo parameterization schemes.

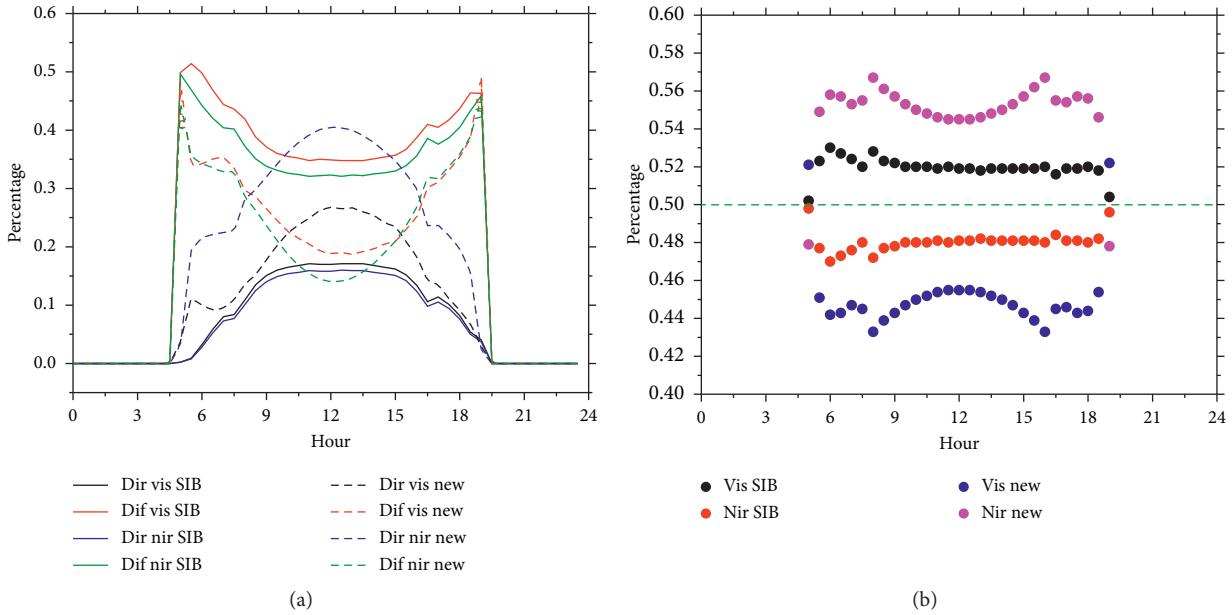

(a) (b)

Figure 4: Comparison of the annual averaged diurnal cycle of the solar radiation partitioning between the method based on the SiB3 and the new surface albedo parameterization schemes. (a) Direct visible radiation, diffuse visible radiation, direct near-infrared radiation, and diffuse near-infrared radiation. (b) Total visible and near-infrared radiation.

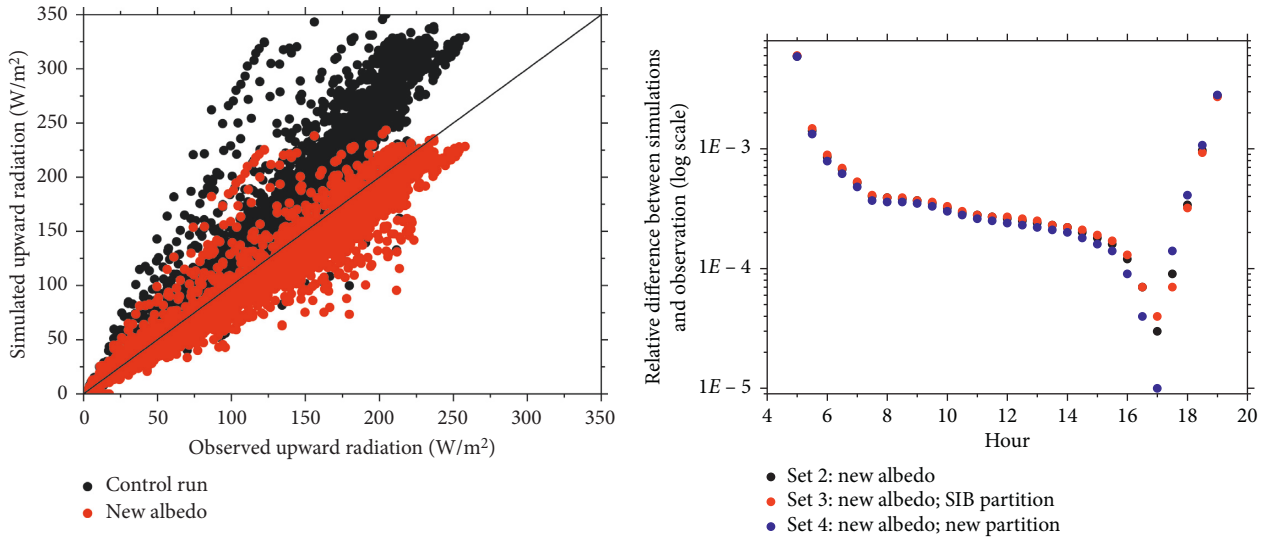

(a) (b)

Figure 5: (a) Comparison of the simulated upward solar radiations for the control run and the set 2 with those of the observations for the whole year. (b) Annual averaged diurnal cycle of the relative differences between the simulated upward solar radiations for the set 2, set 3, and set 4 with those of the observations.

Table 2: Biases, mean errors (MEs), root mean square errors (RMSEs), and correlation coefficients (Rs) of the upward solar radiation simulated by the four sets of experiments compared with those of the observations for the whole year.

	Biases (W/m^2)	MEs (W/m^2)	RMSEs (W/m^2)	Rs
Set 1 (control run)	14.13	14.55	27.95	0.9899
Set 2	−4.58	5.86	11.55	0.9904
Set 3	−4.72	5.96	11.66	0.9905
Set 4	−4.19	5.56	11.17	0.9906

Table 3: Biases, mean errors (MEs), root mean square errors (RMSEs), and correlation coefficients (Rs) of the upward solar radiation simulated by the four sets of experiments compared with those of the observations for each season.

Seasons	Sets	Biases (W/m^2)	MEs (W/m^2)	RMSEs (W/m^2)	Rs
Spring	Set 1 (control run)	14.09	16.53	27.41	0.9947
	Set 2	−8.41	8.68	13.90	0.9945
	Set 3	−8.54	8.80	14.05	0.9945
	Set 4	−7.97	8.28	13.37	0.9945
Summer	Set 1 (control run)	23.17	25.04	41.41	0.9875
	Set 2	−2.17	6.55	11.69	0.9873
	Set 3	−2.43	6.68	11.73	0.9873
	Set 4	−1.71	6.33	11.64	0.9873
Autumn	Set 1 (control run)	10.80	13.30	22.51	0.9980
	Set 2	−5.08	5.23	7.76	0.9982
	Set 3	−5.15	5.29	7.86	0.9982
	Set 4	−4.72	4.91	7.25	0.9982
Winter	Set 1 (control run)	4.30	7.10	12.08	0.9941
	Set 2	−6.63	6.92	12.35	0.9932
	Set 3	−6.74	7.01	12.51	0.9932
	Set 4	−6.33	6.64	11.90	0.9932

In general, for the default surface albedo scheme, the simulated upward solar radiation is larger than the observation. After using the new surface albedo parameterization scheme, in general, the simulated upward solar radiation is decreased and lower than that of the observation. The simulation result is improved definitely compared with the observation; the absolute bias is reduced almost 70%. The mean error and root mean square error are all reduced too. As the total albedo based on the SiB3 solar partitioning method is smaller than that based on the IUM default solar partitioning method, the SiB3-based solar radiation partitioning method could not improve but deteriorate the simulation result. The new solar radiation partitioning method could improve the simulation result, but the range is relatively small; the bias is reduced about 8.5%. However, the solar radiation partitioning mechanism study is still important to land surface radiation and energy balance research.

Then, we compared the simulated upward solar radiation for these four sets of experiments with those of the observations for the four seasons. Table 3 lists the statistical variables of the upward solar radiation simulated by these four sets of experiments compared with those of the observations for each seasons. After using the new surface albedo parameterization scheme, the simulation result is improved in spring, summer, and autumn but deteriorated in winter. The improvement range is the largest in summer; the absolute bias is reduced almost 91%. In winter, the new surface albedo is too small. Compared with the default solar radiation partitioning method, the SiB3-based solar radiation partitioning method deteriorates the simulation results in all the four seasons. On the contrary, the new solar radiation partitioning method improves the simulation results in all the four seasons.

4. Conclusions

In this paper, a surface albedo parameterization scheme was introduced and a solar radiation partitioning method was developed to improve the simulation of the upward solar radiation. The simulation results were validated in a hinterland site of the Taklimakan Desert. The results indicate the surface albedo parameterization scheme is important to parameterize the total surface albedo and upward solar radiation. For the whole year, after using the new surface albedo parameterization scheme, the absolute bias is reduced about 70%. The seasonal analysis indicates the new surface albedo parameterization method could improve the simulation in spring, summer, and autumn. In summer, the absolute bias is reduced about 91%. As for the solar radiation partitioning, the total albedo only depends on the partitioning of the total visible and near-infrared radiations. The new solar radiation partitioning method could improve the simulation result; the bias is reduced about 8.5%. As the surface albedo is a key parameter in surface radiation and energy balance, the findings of this paper could be used in land surface modeling and land-atmospheric interaction research especially in arid and semiarid areas.

In the near future, more sites should be used to validate the universality of the surface albedo parameterization scheme. The observed four components of solar radiation should be used to validate the solar radiation partitioning methods. The visible direct, visible diffuse, near-infrared direct, and near-infrared diffuse radiation data retrieved from Moderate-Resolution Imaging Spectroradiometer (MODIS) [35, 36] should be assimilated into the IUM to expand the application of the solar radiation partitioning method to the regional and global scale.

Data Availability

The observational data from the Tazhong station are from the Institute of Desert Meteorology, China Meteorological Administration, and are available upon request to the corresponding author via e-mail: clmeng@ium.cn.

Conflicts of Interest

The authors declare that they have no conflicts of interest.

Acknowledgments

This work was supported by the National Natural Science Foundation of China under grant 41875125. The authors thank the Institute of Desert Meteorology, China Meteorological Administration, for the Tazhong site observation data.

References

[1] J. Zhai, R. Liu, J. Liu, G. Zhao, and L. Huang, "Radiative forcing over China due to albedo change caused by land cover change during 1990–2010," *Journal of Geographical Sciences*, vol. 24, no. 5, pp. 789–801, 2014.

[2] B. A. Wielicki, T. Wong, N. Loeb et al., "Changes in earth's albedo measured by satellite," *Science*, vol. 308, no. 5723, p. 825, 2005.

[3] E. Burakowski, A. Tawfik, A. Ouimette et al., "The role of surface roughness, albedo, and Bowen ratio on ecosystem energy balance in the Eastern United States," *Agricultural and Forest Meteorology*, vol. 249, pp. 367–376, 2018.

[4] G. L. Potter, H. W. Ellsaesser, M. C. MacCracken, and J. S. Ellis, "Albedo change by man: test of climatic effects," *Nature*, vol. 291, no. 5810, pp. 47–49, 1981.

[5] A. Ellis and M. F. Wilson, "Surface albedo data for climatic modeling," *Reviews of Geophysics*, vol. 21, no. 8, pp. 1743–1778, 1983.

[6] K. Laval and L. Picon, "Effect of a change of the surface albedo of the sahel on climate," *Journal of the Atmospheric Sciences*, vol. 43, no. 21, pp. 2418–2429, 1986.

[7] B. M. Lofgren, "Surface albedo-climate feedback simulated using two-way coupling," *Journal of Climate*, vol. 8, no. 10, pp. 2543–2562, 1995.

[8] A. Hall, "The role of surface albedo feedback in climate," *Journal of Climate*, vol. 17, no. 7, pp. 1550–1568, 2004.

[9] M. Winton, "Surface albedo feedback estimates for the AR4 climate models," *Journal of Climate*, vol. 19, no. 3, pp. 359–365, 2006.

[10] R. A. Colman, "Surface albedo feedbacks from climate variability and change," *Journal of Geophysical Research: Atmospheres*, vol. 118, no. 7, pp. 2827–2834, 2013.

[11] J. A. Crook and P. M. Forster, "Comparison of surface albedo feedback in climate models and observations," *Geophysical Research Letters*, vol. 41, no. 5, pp. 1717–1723, 2014.

[12] G. L. Stephens, D. O'Brien, P. J. Webster, P. Pilewski, S. Kato, and J.-l. Li, "The albedo of earth," *Reviews of Geophysics*, vol. 53, no. 1, pp. 141–163, 2015.

[13] Y. Li, T. Wang, Z. Zeng, S. Peng, X. Lian, and S. Piao, "Evaluating biases in simulated land surface albedo from CMIP5 global climate models," *Journal of Geophysical Research: Atmospheres*, vol. 121, no. 11, pp. 6178–6190, 2016.

[14] A. Schneider, M. Flanner, and J. Perket, "Multidecadal variability in surface albedo feedback across CMIP5 models," *Geophysical Research Letters*, vol. 45, no. 4, pp. 1972–1980, 2018.

[15] A. Sellers and A. J. Meadows, "Long term variations in the albedo and surface temperature of the earth," *Nature*, vol. 254, no. 5495, p. 44, 1975.

[16] L. Berkofsky, "The effect of variable surface albedo on the atmospheric circulation in desert regions," *Journal of Applied Meteorology*, vol. 15, no. 11, pp. 1139–1144, 1976.

[17] M. F. Courel, R. S. Kandel, and S. I. Rasool, "Surface albedo and the Sahel drought," *Nature*, vol. 307, no. 5951, pp. 528–531, 1984.

[18] R. D. Jackson, S. B. Idso, and J. Otterman, "Surface albedo and desertification," *Science*, vol. 189, no. 4207, pp. 1012–1015, 1975.

[19] Y. Otterman, X. Zeng, R. E. Dickinson et al., "The common land model," *Bulletin of the American Meteorological Society*, vol. 84, no. 8, pp. 1013–1024, 2003.

[20] L. C. Nkemdirim, "A note on the albedo of surfaces," *Journal of Applied Meteorology*, vol. 11, no. 5, pp. 867–874, 1972.

[21] K. Wang, P. Wang, J. Liu, M. Sparrow, S. Sparrow, and X. Zhou, "Variation of surface albedo and soil thermal parameters with soil moisture content at a semi-desert site on the western Tibetan Plateau," *Boundary-Layer Meteorology*, vol. 116, no. 1, pp. 117–129, 2005.

[22] Y. Bao, S. Lü, Y. Zhang, X. Meng, and S. Yang, "Improvement of surface albedo simulations over arid regions," *Advances in Atmospheric Sciences*, vol. 25, no. 3, pp. 481–488, 2008.

[23] H. Liu, B. Wang, and C. Fu, "Relationships between surface albedo, soil thermal parameters and soil moisture in the semi-arid area of Tongyu, Northeastern China," *Advances in Atmospheric Sciences*, vol. 25, no. 5, pp. 757–764, 2008.

[24] F. Yang, K. Mitchell, Y.-T. Hou et al., "Dependence of land surface albedo on solar zenith angle: observations and model parameterization," *Journal of Applied Meteorology and Climatology*, vol. 47, no. 11, pp. 2963–2982, 2008.

[25] X. Guan, J. Huang, N. Guo, J. Bi, and G. Bi, "Variability of soil moisture and its relationship with surface albedo and soil thermal parameters over the Loess Plateau," *Advances in Atmospheric Sciences*, vol. 26, no. 4, pp. 692–700, 2009.

[26] Y. Liu, Q. He, H. Zhang, and A. Mamtimin, "Improving the CoLM in Taklimakan desert hinterland with accurate key parameters and an appropriate parameterization scheme," *Advances in Atmospheric Sciences*, vol. 29, no. 2, pp. 381–390, 2012.

[27] S. C. Mamtimin, Z. Wang, and S. Z. Yang, "Parameterization of land surface albdeo," *Chinese Optics Letters*, vol. 12, no. 11, pp. 110101–110105, 2014.

[28] Z. Zheng, W. Dong, Z. Li et al., "Observational study of surface spectral radiation and corresponding albedo over Gobi, desert, and bare loess surfaces in northwestern China," *Journal of Geophysical Research: Atmospheres*, vol. 120, no. 3, pp. 883–896, 2015.

[29] Z. Zheng, Z. Wei, Z. Wen et al., "Inclusion of solar elevation angle in land surface albedo parameterization over bare soil surface," *Journal of Advances in Modeling Earth Systems*, vol. 9, no. 8, pp. 3069–3081, 2017.

[30] A. Weiss and J. M. Norman, "Partitioning solar radiation into direct and diffuse visible and near-infrared components," *Agricultural and Forest Meteorology*, vol. 34, no. 2-3, pp. 205–213, 1985.

[31] P. J. Sellers, Y. Mintz, Y. C. Sud, and A. Dalcher, "A simple biosphere model (SiB) for use within general circulation models," *Journal of the Atmospheric Sciences*, vol. 43, no. 6, pp. 505–531, 1986.

[32] P. J. Dalcher, D. A. Randall, G. J. Collatz et al., "A revised land surface parameterization (SiB2) for atmospheric GCMs. Part 1: model formulation," *Journal of Climate*, vol. 9, no. 4, pp. 676–705, 1996.

[33] P. J. Sellers, C. J. Tucker, G. J. Collatz et al., "A revised land surface parameterization (SiB2) for atmospheric GCMs. Part 2: the generation of global fields of terrestrial biophysical parameters from satellite data," *Journal of Climate*, vol. 9, no. 4, pp. 706–737, 1996.

[34] C. Meng, "The integrated urban land model," *Journal of Advances in Modeling Earth Systems*, vol. 7, no. 2, pp. 759–773, 2015.

[35] L. Zhou, R. E. Dickinson, Y. Tian et al., "Comparison of seasonal and spatial variations of albedos from moderate-resolution imaging spectroradiometer (MODIS) and common land model," *Journal of Geophysical Research*, vol. 108, no. D15, p. 4488, 2003.

[36] A. Cescatti, B. Marcolla, S. K. Santhana Vannan et al., "Intercomparison of MODIS albedo retrievals and in situ measurements across the global FLUXNET network," *Remote Sensing of Environment*, vol. 121, pp. 323–334, 2012.